Support information

Solvation-Driven Interphase Engineering and Mechanical Failure Pathways in Large-Scale Anode-Free Lithium Metal Batteries

Nattanon Joraleechanchai, Nuttida Matkhaw, Thitiphum Sangsanit, Worapol Tejangkura and Montree Sawangphruk*

Centre of Excellence for Energy Storage Technology (CEST), Department of Chemical and Biomolecular Engineering, School of Energy Science and Engineering, Vidyasirimedhi Institute of Science and Technology, Rayong 21210, Thailand

* Corresponding author

E-mail address: montree.s@vistec.ac.th (M. Sawangphruk).

Table S1. Checklist of battery cell fabrication and testing.

Table I. information checklist	
Electrode and cells	
Cell type and configuration	18650 anode free configuration
Electrode's geometry and size	Cathode: length 100 cm. width 5.6 cm. Anode: length 105 cm. width 5.8 cm.
Description of electrode preparation (including post-coating treatments such as compression/calendering)	Cathode mixing ratio: 95.2: 2.4: 2.4 (active mass: Super P: PVDF) at 70 - 2,000 rpm for 12 hours. Solvent evaporation: 145 °C Calendering force: 6 tons
Electrode's active material areal mass loading (or areal capacity)	Cathode: 20.67 ± 0.47 g/electrode ~ 36.91 mg/cm² for double-sided coating and 18.45 mg/cm² for single-sided coating.
Composition of the electrodes, including supplier and purity of pursued components	95.2 wt.% Active materials: NMC90 and Li_2NiO_2 from Gelon (China) 2.4 wt.% Binder: PVDF from Gelon (China) 2.4 wt.% Conductive additive: Super P from Gelon (China) Battery grade (< 20 PPM moisture impurity)

Table I. information checklist	
Apparent electrode density (calculated as the ratio of areal mass loading and thickness)	2.46 g/cm3
Current collector type and thickness (if not flat, also weight)	Cathode: Al foil with 14 um thickness Anode: Cu foil with 6.8 um thickness
Separator type & thickness	Al_2O_3 coated PP/PE/PP & 16 um from Yunji (China)
Electrolyte composition and volume/weight used in the cell	1.2 M $LiPF_6$ FEC:DEC (1:4) 1.2 M $LiPF_6$ FEC:DEC:TTE (2:6:2) 1.2 M $LiPF_6$ FEC:DEC:TTE (2:4:4) 1.2 M $LiPF_6$ FEC:DEC:TTE (2:3:5) 4.68 ± 0.14 g per 18650 cells
Electrochemical testing	
Testing temperature	Room temperature (25°C)
Voltage (or potential) range	Formation cycle: 3.0 – 4.3 V Stability and rate performance: 3.0 – 4.3 V
Theoretical capacity and specified C-rate	1 C = 3,600 mAh/cell, 212 mAh/g of NMC
Charge / discharge program (CC, CV, combination)	CCCV charge and CC discharge
C-rate for each electrochemical measurement	From C/10 – 1C rate
Initial electrochemical profile	78.33% (coin-cell) 71.4-83.5% (18650)

Table II. Performance Reporting			
Cell type	Coin cell	Pouch cell	Other
Cell configuration	2-electrode cell	3-electrode cell	
Mass loading of active material	<2 mg cm^{-2}		
	2-5 mg cm^{-2}		
	5-8 mg cm^{-2}		
	>8 mg cm^{-2}		
	Cathode: 20.67 ± 0.47 g/electrode ~ 36.91		

Table I. information checklist		
	mg/cm² for double-sided coating and 18.45 mg/cm² for single-sided coating.	
Number of cycles	Metal anode/battery (incl. half cells)	Full cell
	<50	Capacity Retention: 80% after 50 cycles, tested at C/2 CCCV charge and 1C CC discharge rates.
	50-200	

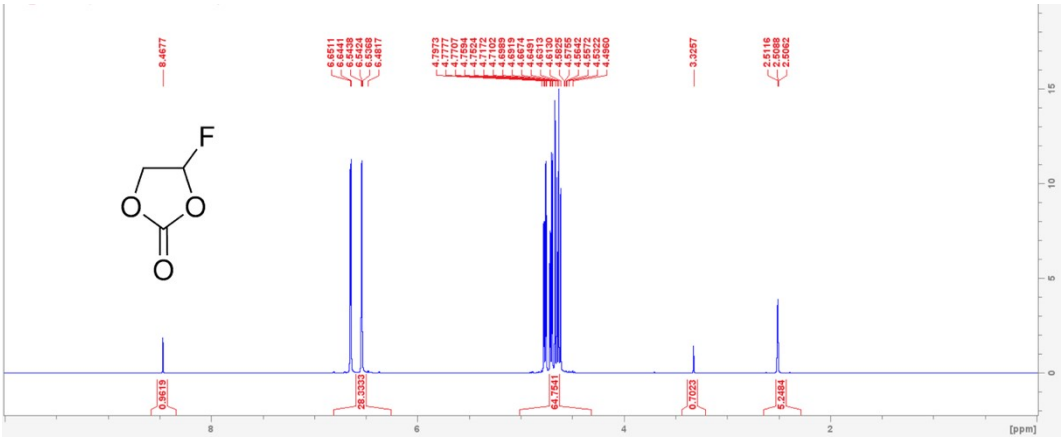

Figure S1. ^{1}H NMR of Fluoroethylene carbonate (FEC)

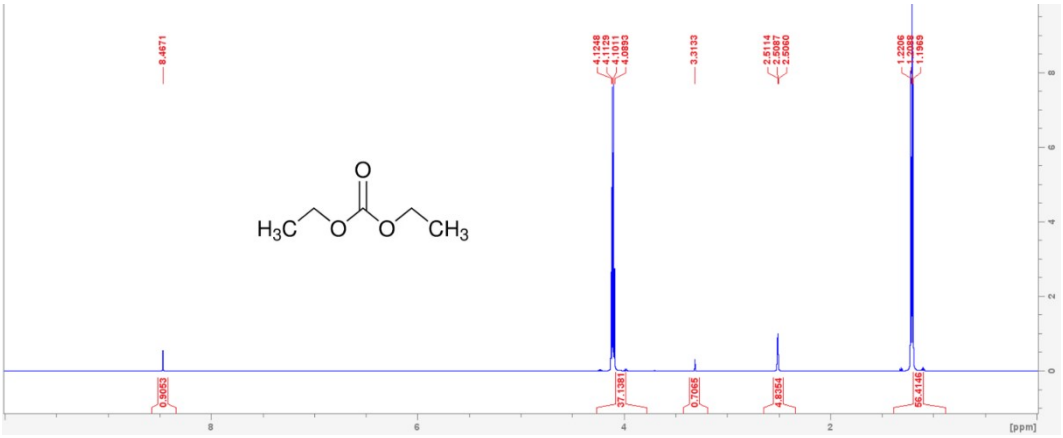

Figure S2. ^{1}H NMR of diethyl carbonate (DEC)

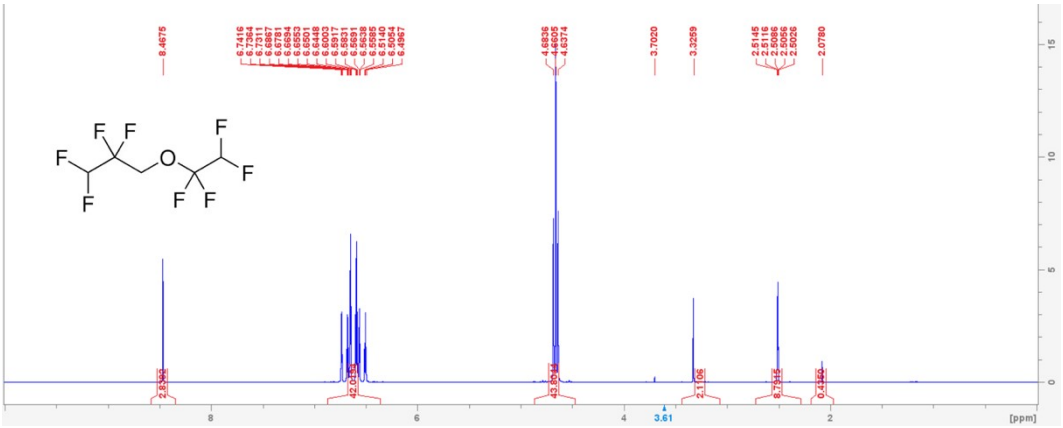

Figure S3. ^{1}H NMR of 1,1,2,2-tetrafluoroethyl 2,2,3,3-tetrafluoropropyl ether (TTE)

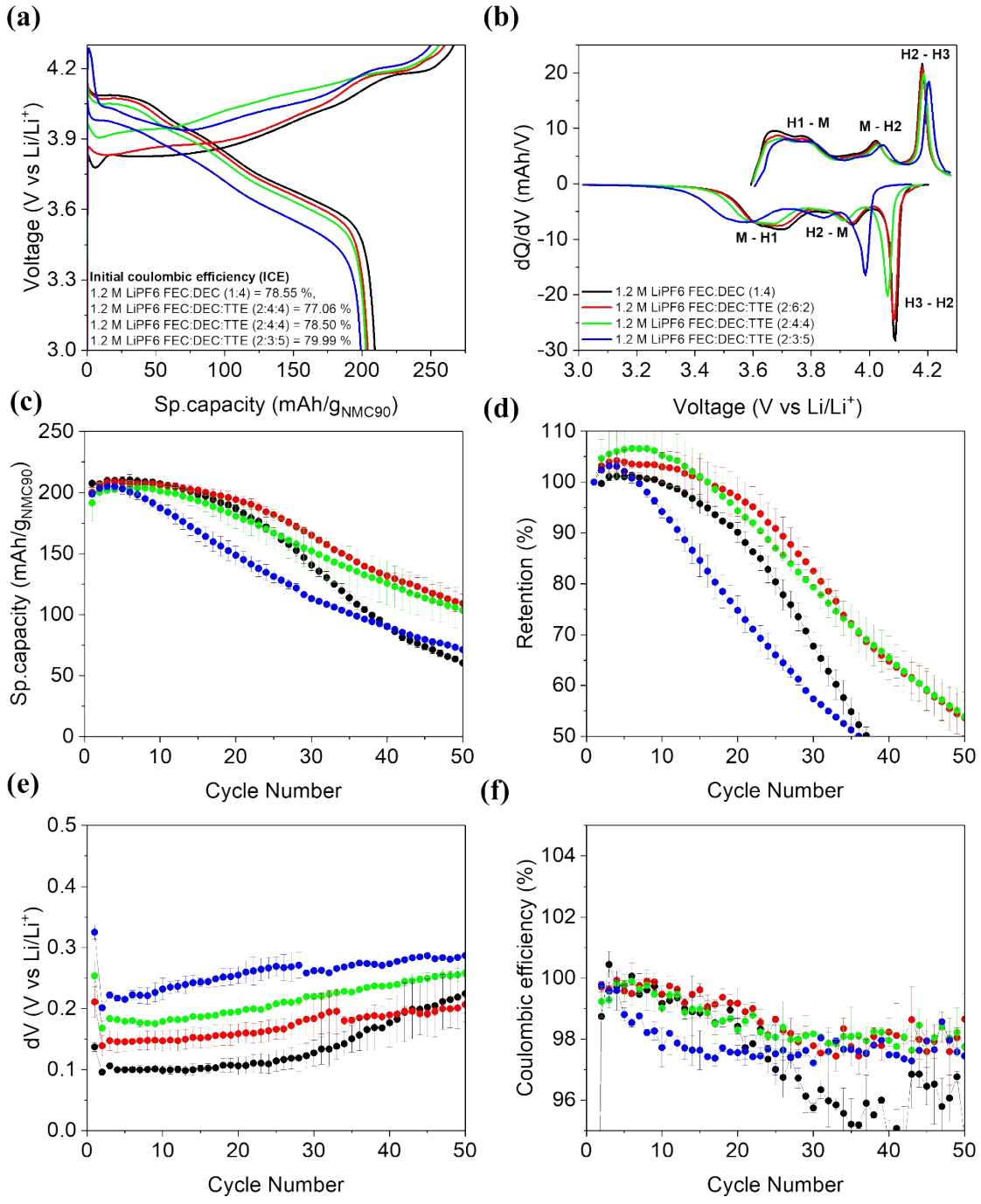

Figure S4. Electrochemical characterization of anode-free NMC90+Li_2NiO_2 coin-cells with varying FEC:DEC:TTE electrolyte formulations. (a) Charge-discharge voltage profiles. (b) Corresponding differential capacity (dQ/dV) plots. (c) Specific capacity, (d) Capacity retention (e) Polarization growth, and (f) Coulombic efficiency (CE) of cycling performance at 0.2C CCCV-charge and 0.5C CC-discharge.

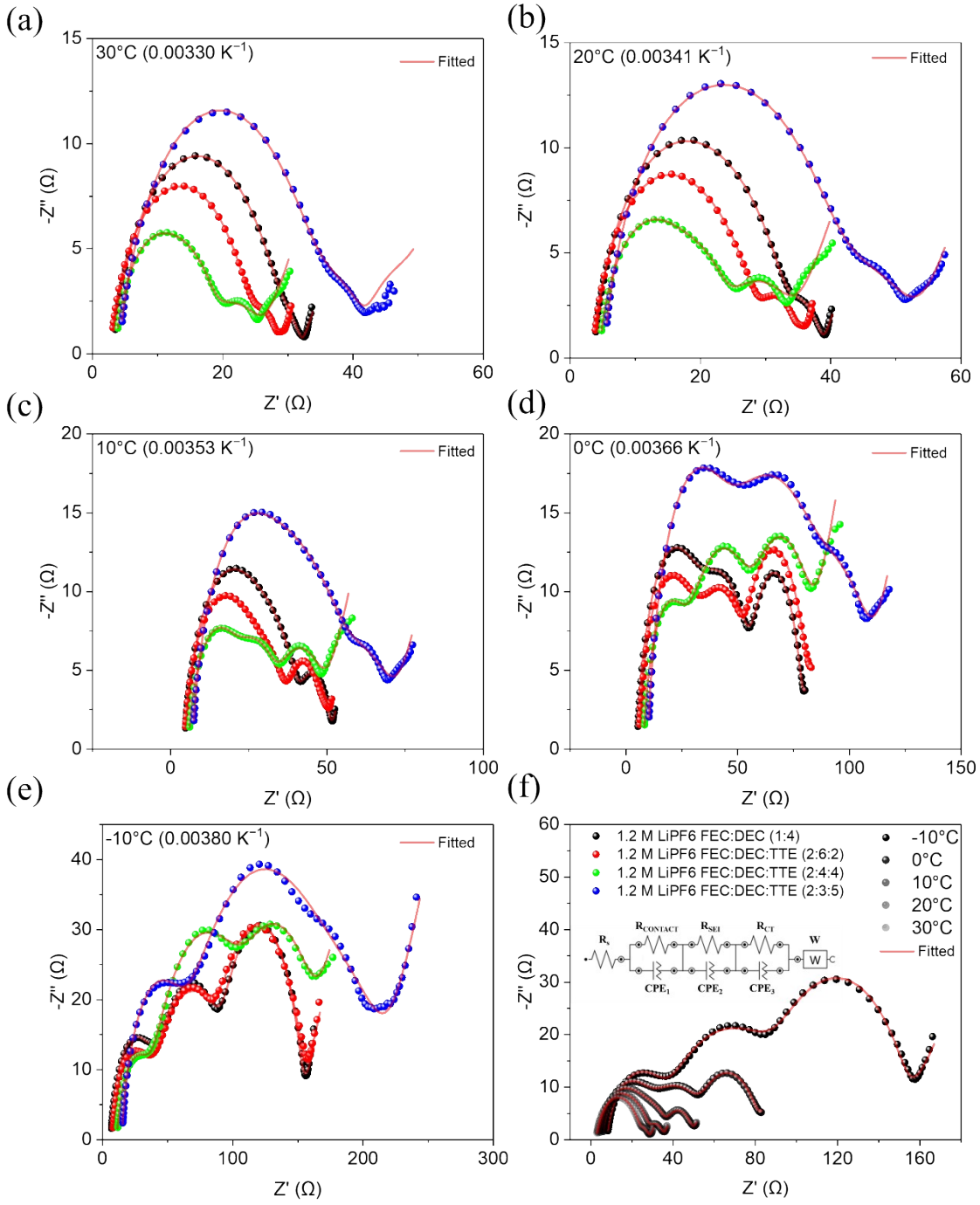

Figure S5. Nyquist plots and corresponding fitted data of Cu‖NMC90+LNO CR2032 coin cells. Panels (a–e) present the impedance spectra collected at 30 °C, 20 °C, 10 °C, 0 °C, and −10 °C for electrolytes with different FEC:DEC:TTE ratios. (f) The examples of fitted Nyquist plots of Cu‖NMC90+LNO CR2032 coin cells using the corresponding equivalent circuit model.

Table S2. Temperature-dependent impedance parameters obtained from equivalent circuit fitting of Cu‖NMC90 coin cells using electrolytes with different FEC:DEC:TTE ratios. The parameters include the solution resistance (R_S), contact resistance ($R_{CONTACT}$), SEI resistance (R_{SEI}), charge-transfer resistance (R_{CT}), and the total interfacial resistance (R_{SUM} = Rcontact + R_{SEI} + R_{CT}), measured from 30 °C to −10 °C. All resistance values are reported in Ω cm⁻².

Electrolyte	Temp °C	R_S Ω. cm-2	$R_{CONTACT}$ Ω. cm-2	R_{SEI} Ω. cm-2	R_{CT} Ω. cm-2	R_{SUM} Ω. cm-2
1.2 M LiPF6 FEC:DEC (1:4)	30	2.79	16.62	5.31	3.50	25.43
	20	3.13	14.14	12.29	4.39	30.82
	10	3.79	18.83	14.14	7.95	40.92
	0	4.31	23.69	22.01	18.65	64.34
	-10	5.59	28.55	49.05	49.49	127.10
1.2 M LiPF6 FEC:DEC:TTE (2:6:2)	30	2.42	13.79	4.78	4.22	22.79
	20	3.04	12.20	9.90	5.93	28.03
	10	3.78	16.09	12.90	10.34	39.33
	0	4.99	19.62	23.86	22.01	65.49
	-10	6.86	24.31	49.49	51.97	125.77
1.2 M LiPF6 FEC:DEC:TTE (2:4:4)	30	3.14	9.19	7.56	3.12	19.87
	20	3.95	11.49	9.55	4.97	26.00
	10	5.03	13.43	12.29	11.31	37.03
	0	6.91	16.62	27.13	19.53	63.28
	-10	9.81	22.01	66.20	36.50	124.71
1.2 M LiPF6 FEC:DEC:TTE (2:3:5)	30	3.54	25.90	7.59	3.98	37.47
	20	4.51	17.41	13.70	11.49	42.60
	10	6.06	21.57	18.21	17.32	57.10
	0	8.56	38.36	28.90	20.24	87.50
	-10	13.08	35.35	100.76	38.80	174.91

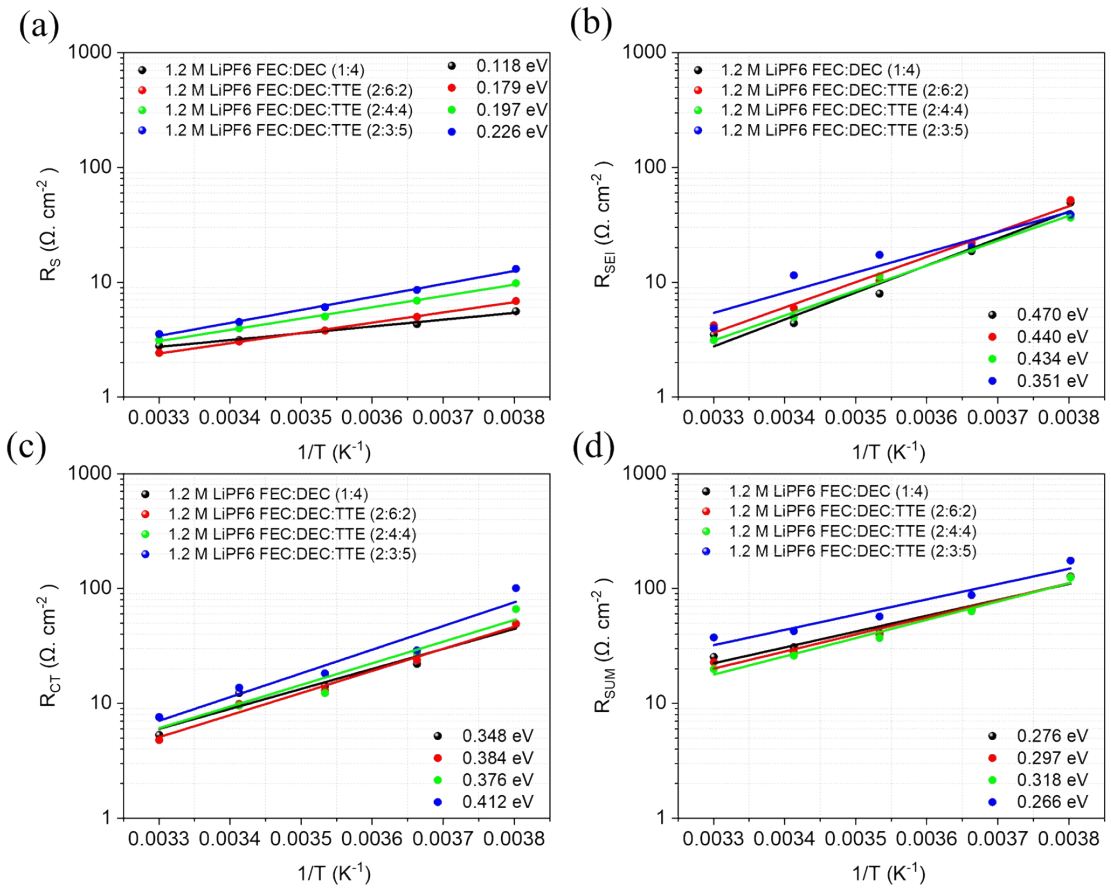

Figure S6. Impedance plotted on a logarithmic scale versus the inverse of temperature for (a) ionic solution resistance (R_S), (b) Interfacial resistance (R_{SEI}), (c) Charge transfer resistance (R_{CT}), and (d) Overall resistance (R_{SUM}).

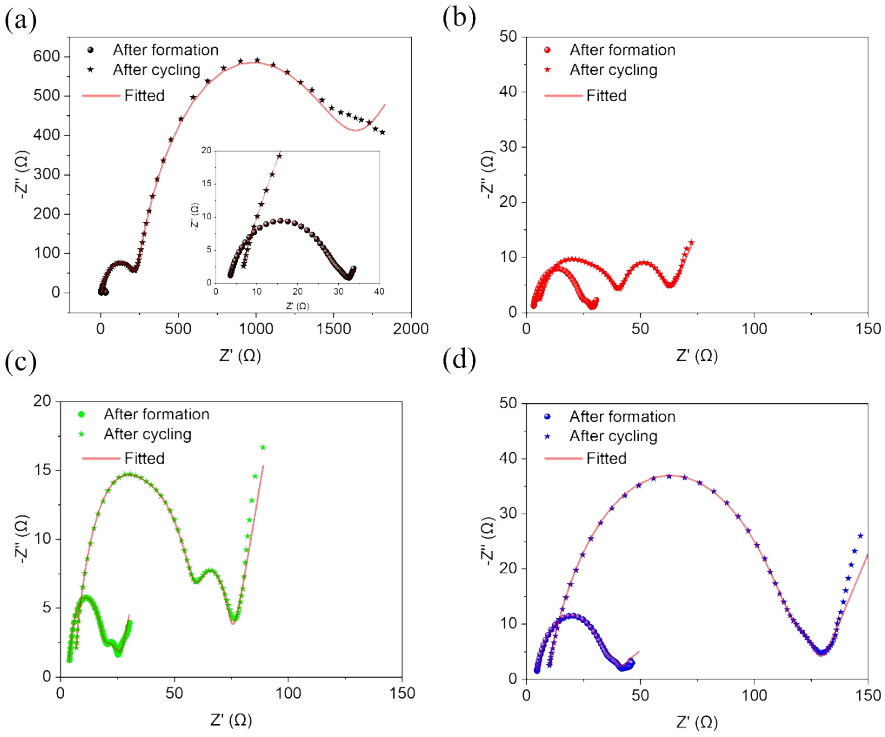

Figure S7. Nyquist plots of Cu‖NMC90+LNO 2032 coin cells measured after formation and after cycling using different electrolyte formulations: (a) 1.2 M $LiPF_6$ in FEC:DEC (1:4); (b) 1.2 M $LiPF_6$ in FEC:DEC:TTE (2:6:2); (c) 1.2 M $LiPF_6$ in FEC:DEC:TTE (2:4:4); and (d) 1.2 M $LiPF_6$ in FEC:DEC:TTE (2:3:5).

Table S3. Extracted values of R_s, R_{SEI}, and R_{ct}obtained from fitting the Nyquist plots of cells with different electrolyte formulations after formation.

After formation	R_S (Ω. cm-2)	$R_{CONTACT}$ (Ω. cm-2)	R_{SEI} (Ω. cm-2)	R_{CT} (Ω. cm-2)
1.2 M LiPF6 FEC:DEC (1:4)	2.79	16.62	5.31	3.50
1.2 M LiPF6 FEC:DEC:TTE (2:6:2)	2.42	13.79	4.78	4.22
1.2 M LiPF6 FEC:DEC:TTE (2:4:4)	3.14	9.19	7.56	3.12
1.2 M LiPF6 FEC:DEC:TTE (2:3:5)	3.54	25.90	7.59	3.98

Table S4. Extracted values of R_s, R_{SEI}, and R_{ct}obtained from fitting the Nyquist plots of cells with different electrolyte formulations after cycling.

After Cycling	R_S (Ω. cm-2)	$R_{CONTACT}$ (Ω. cm-2)	R_{SEI} (Ω. cm-2)	R_{CT} (Ω. cm-2)
1.2 M LiPF6 FEC:DEC (1:4)	4.93	55.77	135.23	1078.28
1.2 M LiPF6 FEC:DEC:TTE (2:6:2)	4.15	19.09	12.90	17.32
1.2 M LiPF6 FEC:DEC:TTE (2:4:4)	5.36	24.92	22.89	12.02
1.2 M LiPF6 FEC:DEC:TTE (2:3:5)	7.93	49.94	46.67	7.95

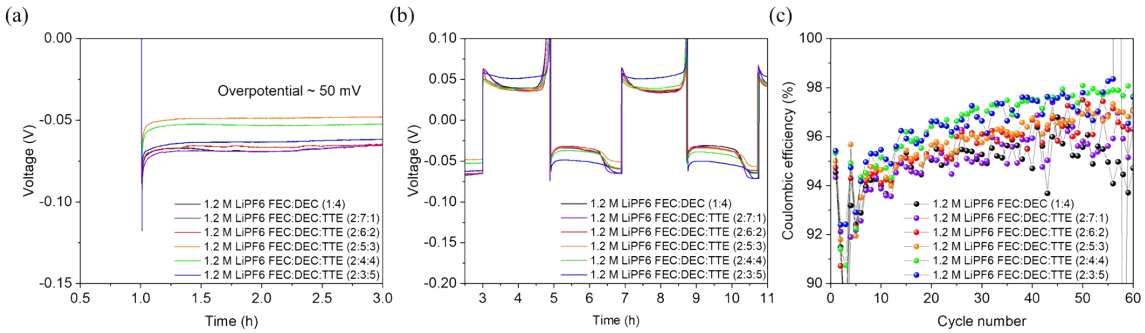

Figure S8. **Electrochemical results of Li/Cu half cells using electrolytes with varying FEC:DEC:TTE ratios.** (a) Lithium nucleation overpotential on copper foil during 1st lithium. (b) Voltage profiles during initial lithium plating/stripping (c) Coulombic efficiency as a function of cycle number, demonstrating enhanced reversibility and more stable lithium deposition in electrolytes containing TTE compared with the baseline electrolyte.

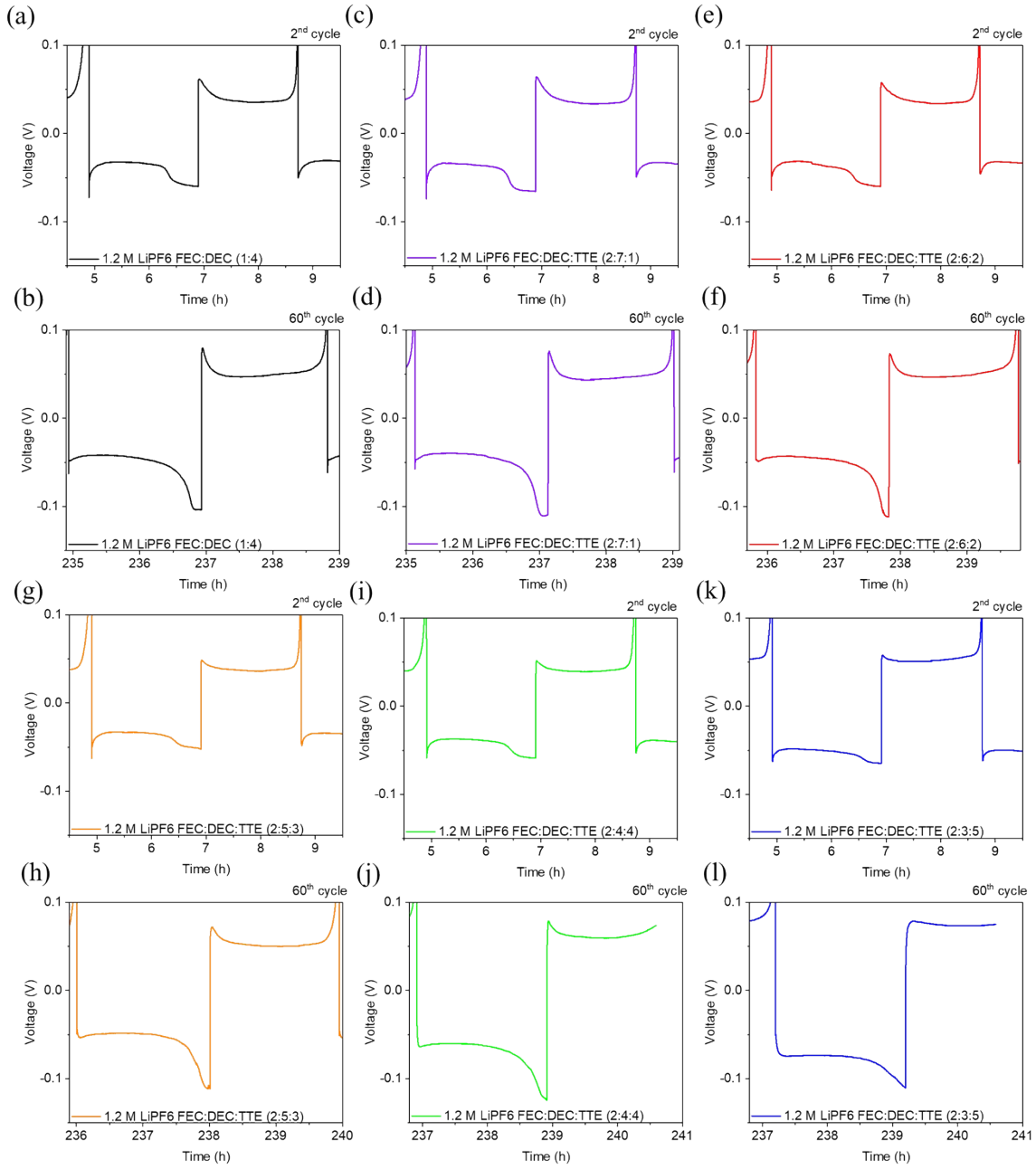

Figure S9. Lithium plating–stripping voltage profiles of Li/Cu half cells with different TTE contents. (a, c, e, g, i, k) show the 2nd cycle for electrolytes containing 0, 10, 20, 30, 40, and 50 vol% TTE, respectively. (b, d, f, h, j, l) show the corresponding 60th cycle for electrolytes containing 0, 10, 20, 30, 40, and 50 vol%.

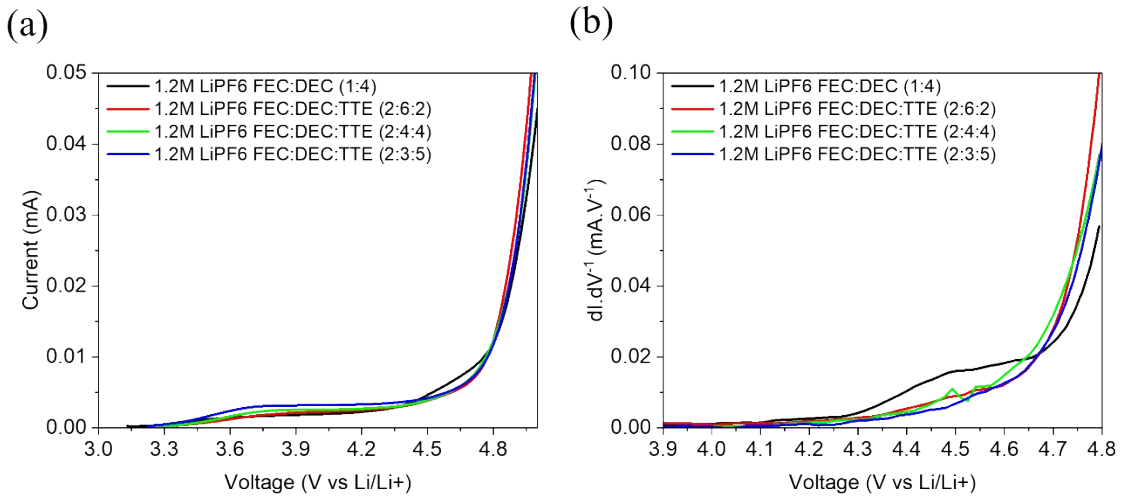

Figure S10. (a) Linear sweep voltammetry (LSV) curves and (b) corresponding dI/dV plots as a function of voltage (up to 5 V) for electrolytes with different FEC:DEC:TTE ratios.

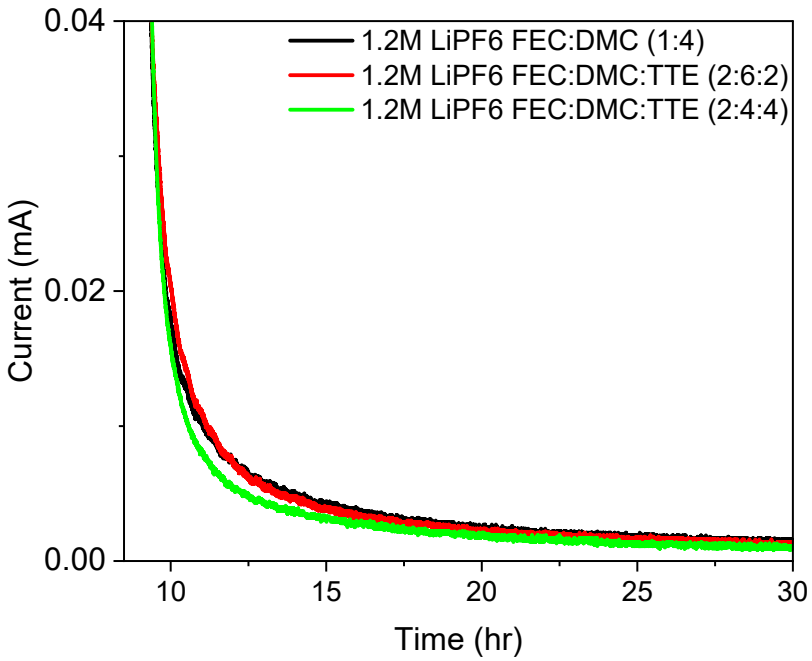

Figure S11. Chronoamperometry profiles at 4.3 V vs. Li/Li$^+$ for 20 h for electrolytes with different FEC:DEC:TTE ratios.

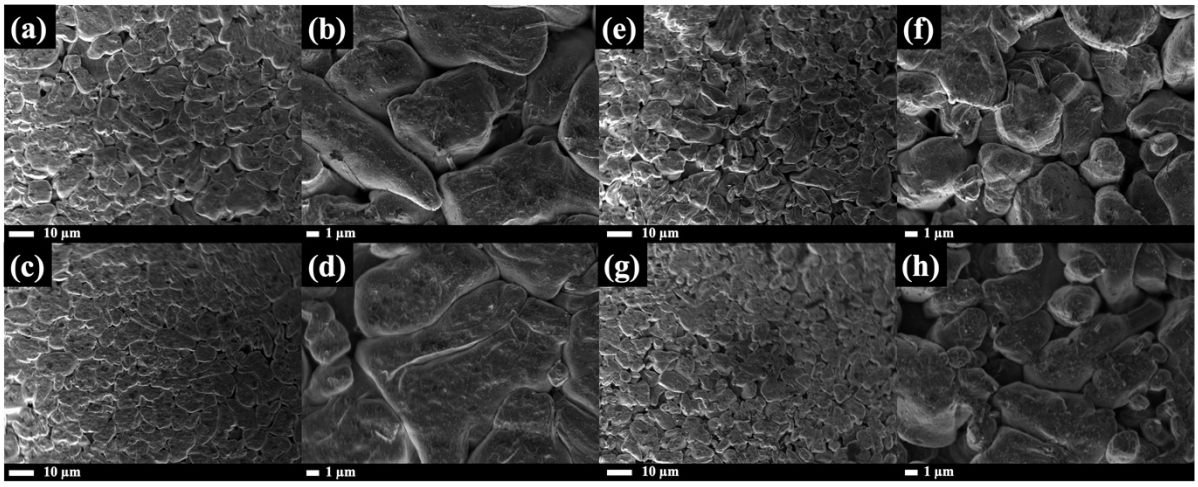

Figure S12. SEM-images of Lithium morphology on copper anode after 1st plating of cell with different electrolyte. (a-b) 1.2 M $LiPF_6$ in FEC:DEC (1:4), (c-d) 1.2 M $LiPF_6$ in FEC:DEC:TTE (2:6:2, (e-f) 1.2 M $LiPF_6$ in FEC:DEC:TTE (2:4:4) , and (g-h) 1.2 M $LiPF_6$ in FEC:DEC:TTE (2:3:5).

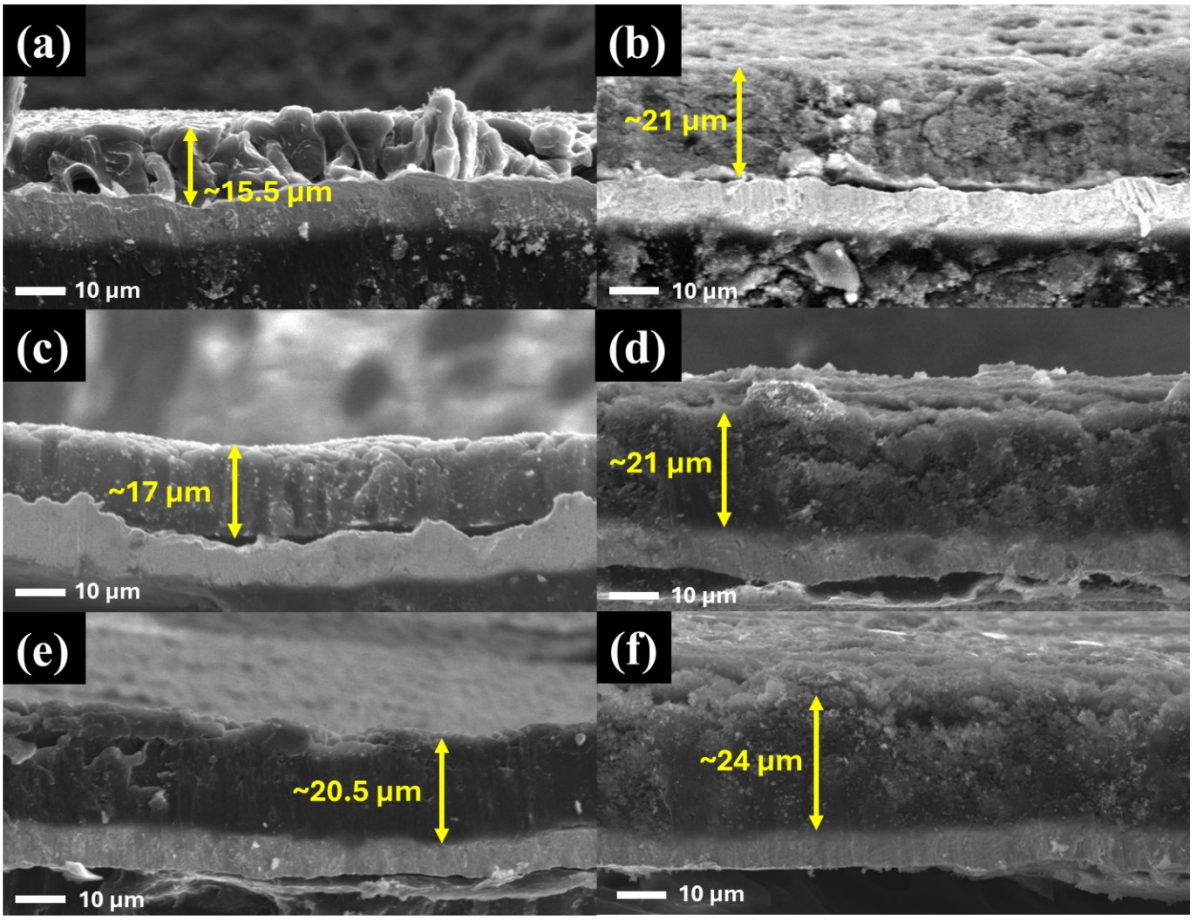

Figure S13. Cross-sectional SEM images of lithium morphology on Cu anodes after the 1st and 20th plating cycles in cells with different electrolyte formulations. (a-b) 1.2 M $LiPF_6$ in FEC:DEC (1:4), (c-d) 1.2 M $LiPF_6$ in FEC:DEC:TTE (2:6:2, and (e-f) 1.2 M $LiPF_6$ in FEC:DEC:TTE (2:3:5).

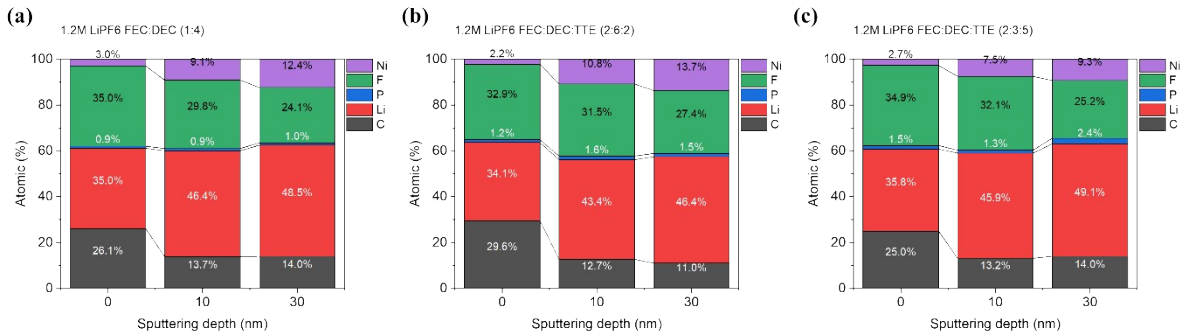

Figure S14. Elemental composition evolution along the sputtering depth by XPS. Stacked bar charts present the depth-resolved atomic percentages of C, O, F, P, and Li in the SEI formed with different electrolyte formulations.

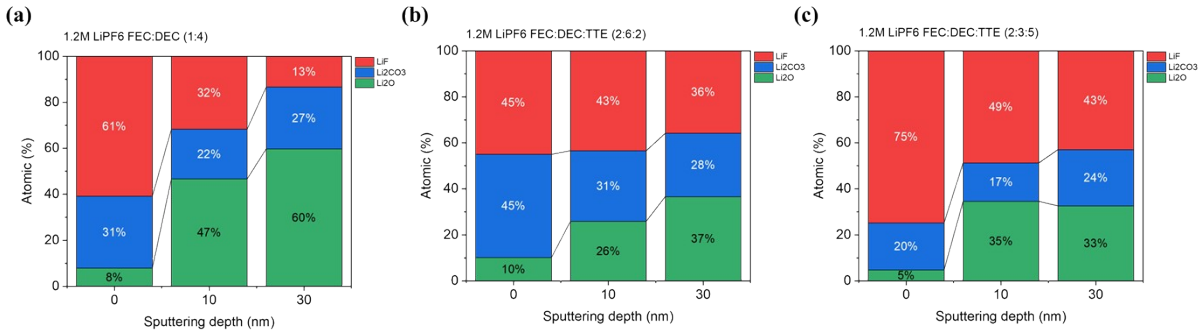

Figure S15. Elemental composition evolution along the sputtering depth by XPS based on Li 1s deconvolution. The relative fractions of LiF, Li_2CO_3, and Li_2O at different sputtering depths are compared for various electrolyte formulations.

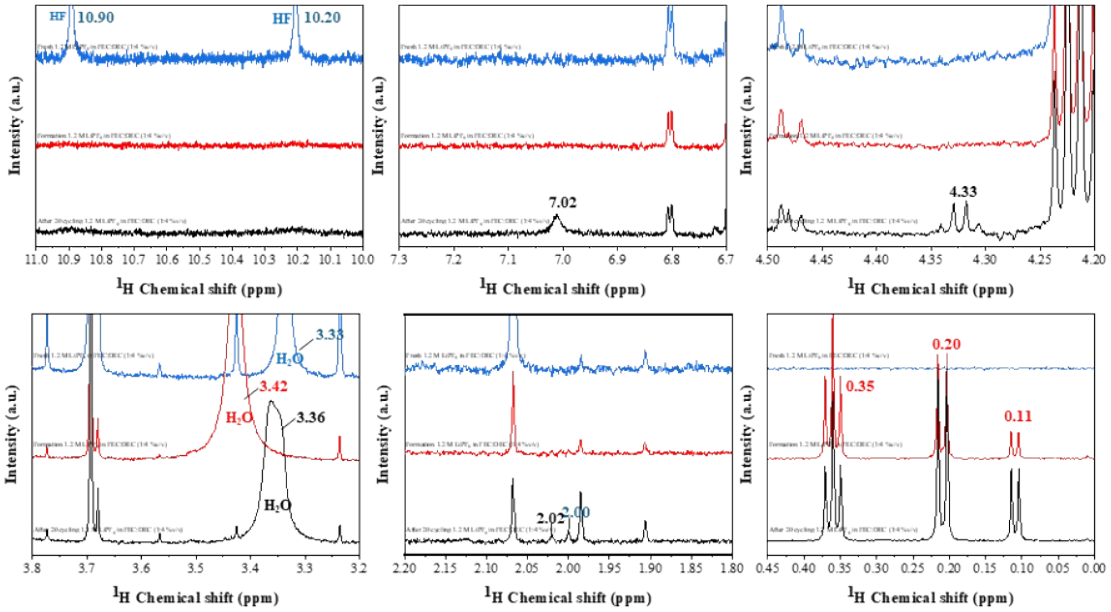

Figure S16. ^{1}H-NMR Spectra of 1.2 M $LiPF_6$ FEC:DEC (1:4). This figure compares the electrolyte composition fresh (blue), after formation (red), and 20 cycles (black). The spectra reveal that key decomposition products present in the baseline electrolyte.

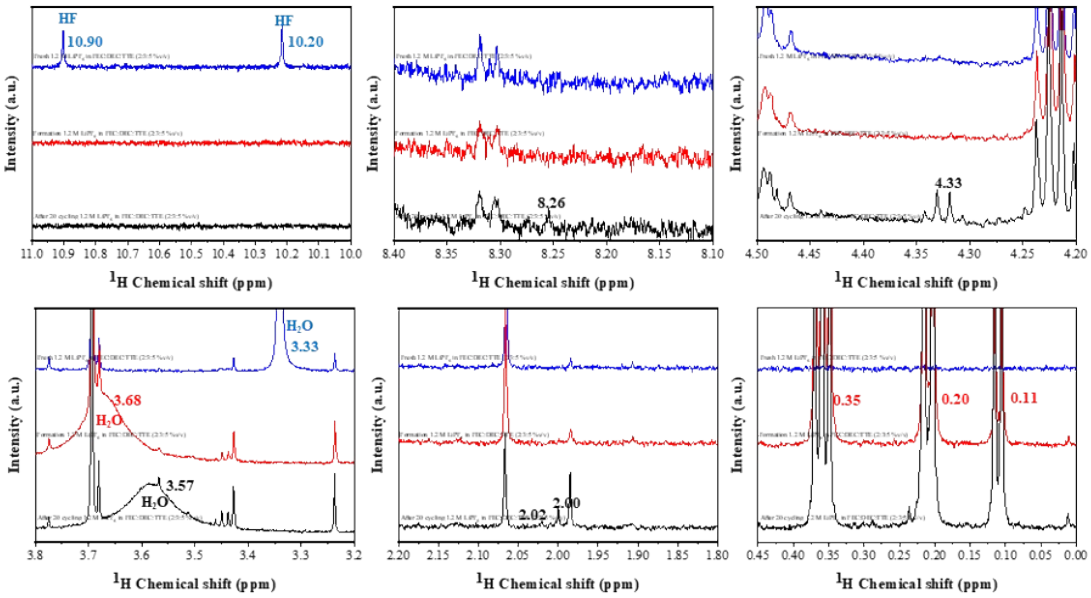

Figure S17. ^{1}H-NMR Spectra of 1.2 M LiPF6 FEC:DEC:TTE (2:3:5). This figure compares the electrolyte composition fresh (blue), after formation (red), and 20 cycles (black). The spectra reveal that key decomposition products present in the 50%TTE contained electrolyte.

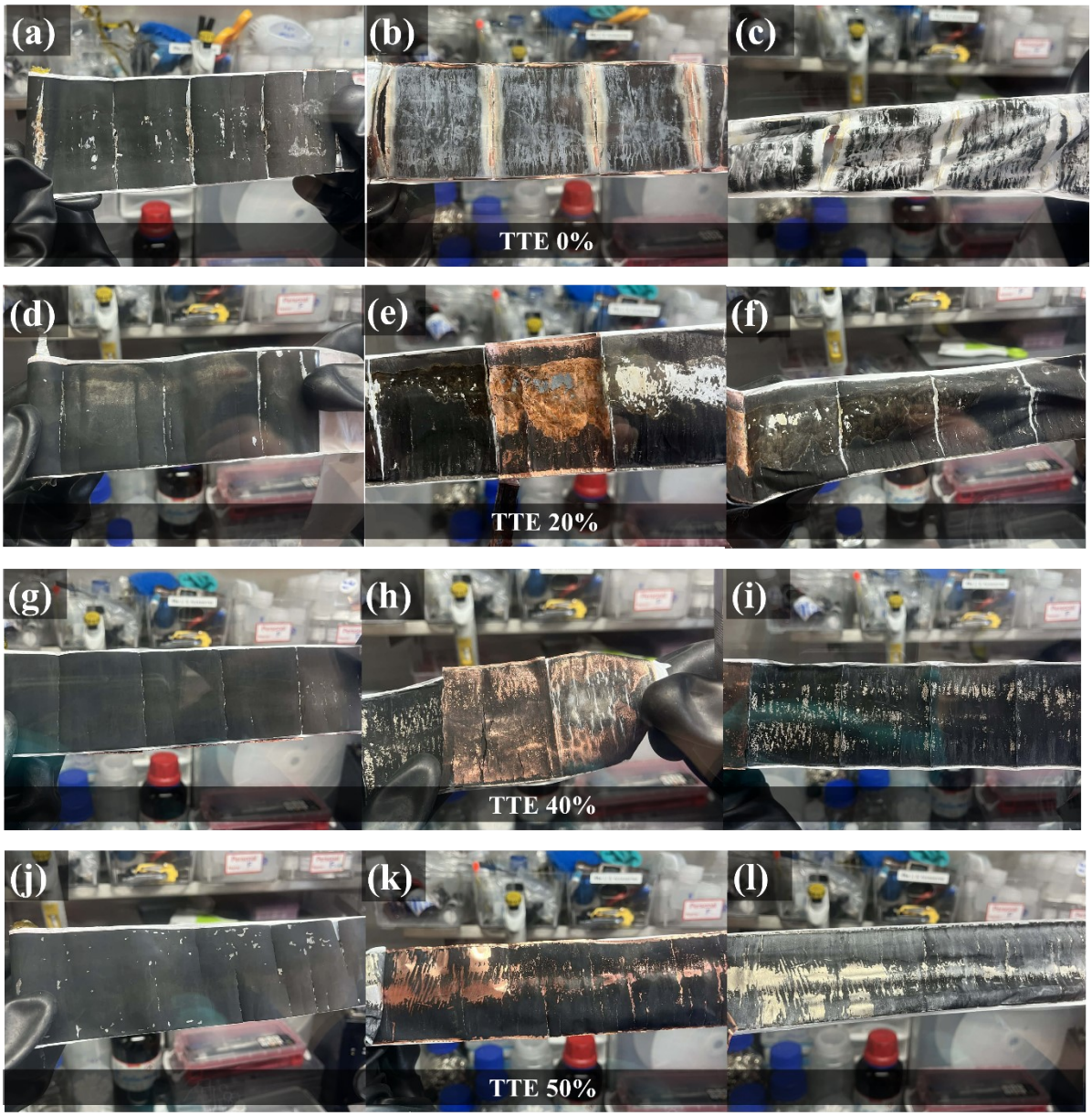

Figure S18. Post-mortem photographs of (left) cathode, (middle) anode, and (right) separator recovered from cycled 18650 anode-free cells employing electrolytes with different TTE contents: (a–c) 0% TTE, (d–f) 20% TTE, (g–i) 40% TTE, and (j–l) 50% TTE. Cells using the TTE-free electrolyte exhibit pronounced electrode deformation, cracking, and severe surface damage after cycling.

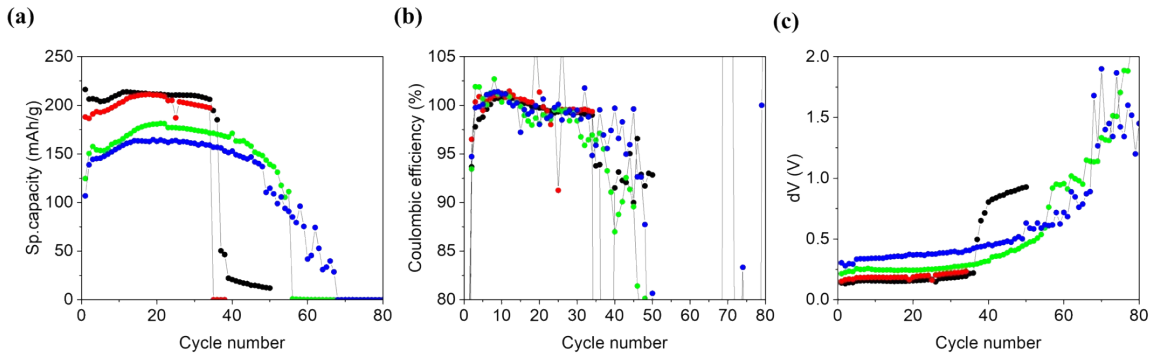

Figure S19. Electrochemical characterization of anode-free NMC90+Li_2NiO_2 18650 cylindrical-cells with varying FEC:DEC:TTE electrolyte formulations cycling at charging rate of C/5 and a discharging rate of D/2. (a) Specific capacity, (b) Polarization growth, and (d) Coulombic efficiency (CE) of cycling performance.

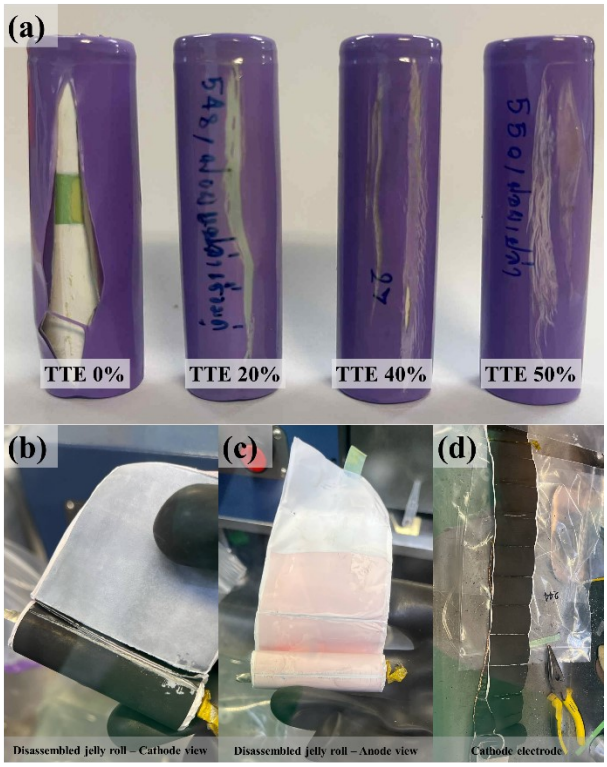

Figure S20. Post-mortem analysis of a cycled 18650 cell after disassembly (charge: C/5; discharge: C/2). (a) post-cycled cells contained different electrolytes. The disassembled jelly roll showing (b) the cathode view, (c) the anode view and (d) anode electrode revealing significant "dead lithium" formation.

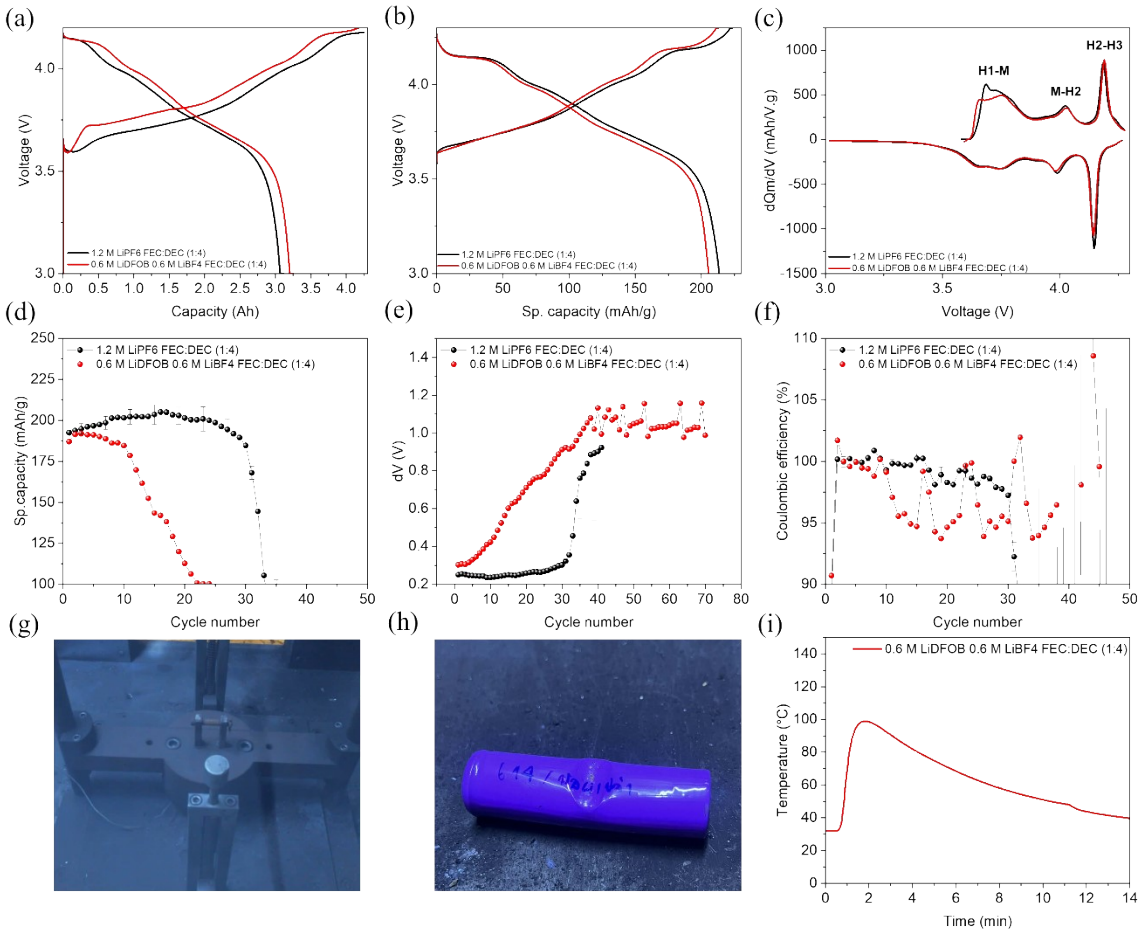

Figure S21. Electrochemical performance and mechanical impact behavior of 18650 anode-free cells during UN38.3 impact testing. (a) First-cycle charge–discharge voltage profiles, (b) specific capacity, (c) differential capacity (dQ/dV) profiles, (d) capacity retention, (e) voltage polarization growth, and (f) Coulombic efficiency, comparing cells using 1.2 M $LiPF_6$ in FEC:DEC (1:4) and 0.6 M LiDFOP + 0.6 M $LiBF_4$ in FEC:DEC (1:4) electrolytes. (g) Results of the UN38.3 mechanical impact test, (h) optical image of the cell after mechanical abuse without explosion or thermal runaway, and (i) temperature evolution as a function of time during the impact test for the cell containing 0.6 M LiDFOP + 0.6 M $LiBF_4$ in FEC:DEC (1:4).

0.6 M LiDFOB 0.6 M LiBF4
FEC:DEC (1:4)

Figure S22. Flammability test of 0.6 M LiDFOB 0.6 M LiBF4 FEC:DEC (1:4)

Table S5. Quantify of Jelly Roll Expansion During Initial Plating.

Cell number	$r_{jelly\ roll\ at\ OCV}$	$r_{jelly\ roll\ at\ 4.3\ V}$	Expansion Δr	Expansion Δr	Estimated expansion critical
	mm	mm	mm	%	mm
1	8.000	8.600	0.600	7.500	-
2	8.125	8.724	0.599	7.380	-
3	8.250	8.858	0.608	7.369	-
4	8.375	8.992	0.617	7.391	0.525
5	8.500	9.125	0.625	7.353	0.408

Table S6. Estimated critical expansion of jelly roll.

Cell No.	$r_{jelly\ roll\ at\ OCV}$	r_{tube}	Gap between jelly roll and tube	Expansion Δr	Estimated expansion critical	r critical	r critical
	mm	mm	mm	mm	mm	mm	%
4	8.375	8.625	0.245	0.617	0.525	0.280	~3.3
5	8.500	8.605	0.105	0.625	0.408	0.303	

Table S7. Radial strain of jelly roll expansion.

Casing	Radial strain due to jelly roll expansion (dimensionless), ε
Borosilicate glass (test tube)	0.033
3A Steel (18650 case)	0.0276

Table S8. Summary observed species from ^{1}H-NMR of Varying FEC:DEC:TTE Electrolyte Formulations.

Electrolyte formulations	Fresh	After formation	After 20th cycle	Species
1.2 M LiPF6 in FEC:DEC (1:4 %v/v)	-	d, 0.11	d, 0.11	Silicone impurity
	-	d, 0.2	d, 0.2	
	-	t, 0.35	t, 0.35	
	-	-	s, 2	Lithium Acetate-Related
	-	-	s, 2.02	
	-	-	q, 4.33	lithium ethyl carbonate (LEC)
	-	-	s, 7.02	VC
	d, ~10.6	-	-	HF
1.2 M LiPF6 in FEC:DEC:TTE (2:4:4 %v/v)	-	d, 0.11	d, 0.11	Silicone impurity
	-	d, 0.2	d, 0.2	
	-	t, 0.35	t, 0.35	
	-	-	s, 2	Lithium Acetate-Related
	-	-	s, 2.02	
	-	-	q, 4.33	lithium ethyl carbonate (LEC)
	-	-	s, 8.26	Formic acid
	d, ~10.6	-	-	HF
1.2 M LiPF6 in FEC:DEC:TTE (2:3:5 %v/v)	-	d, 0.11	d, 0.11	Silicone impurity
	-	d, 0.2	d, 0.2	
	-	t, 0.35	t, 0.35	
	-	-	s, 2	Lithium Acetate-Related
	-	-	s, 2.02	
	-	-	q, 4.33	lithium ethyl carbonate (LEC)
	-	-	s, 8.26	Formic acid
	d, ~10.6	-	-	HF

Supporting VDOs

Flammability test:
https://www.dropbox.com/scl/fo/s3xsj45e6v5n6cckpxayz/AAJ166wCdb9CORWYSWcXi-U?rlkey=wh5m0c50b4w2km0cwwf929szy&dl=0

Impact test:
https://www.dropbox.com/scl/fo/sc7qwa6sglkugywbdcr1h/AGgStHjLVuOqNFmMMvEVtn0?rlkey=ryi3xes29cfbsewjd8vifb7zy&dl=0